Pd and Pt impurity-induced changes in noble-metal density of states: Photoelectron spectroscopy and theory

D. van der Marel,* J. A. Jullianus, and G. A. Sawatzky
Physical Chemistry Department of the Material Science Center, University of Groningen, Nijenborgh 16, 9747 AG Groningen, The Netherlands
(Received 25 March 1985)

High-resolution photoemission results on dilute noble-metal Pd and Pt alloys are presented. The impurity virtual-bound-state widths, splittings, and positions are determined. Using difference techniques we determine the impurity-induced changes in the host-metal d bands and compare these to predictions using a model Hamiltonian. We also discuss the importance of lattice relaxation and show that the neglect of this in first-principles calculations is probably the reason for poor agreement with experiment.

I. INTRODUCTION

Dilute alloys of transition metals dissolved in noble metals are interesting test cases for experimental and theoretical studies of scattering, localization, and correlation problems in solid-state physics.[1–4] Recently, a great deal of theoretical effort has been devoted to developing so-called first-principles methods[5–9] for calculating impurity-induced changes in the density of states, and the local impurity density of states for transition-metal impurities in various metallic hosts. Although these calculations, to some extent, replace the older methods based on model Hamiltonians,[10–13] the latter still provide a clear physical picture for the effects observed especially in systems where local electron correlation effects are of importance. Although the theoretical efforts have been extensive there has been relatively little experimental activity using modern techniques in the area of dilute alloys. The major experimental efforts have concentrated on various forms of transport measurements which provide detailed information on the low-energy-scale (kT) properties of these systems.

Of course, it is the changes in the low-energy-scale behavior upon alloying which directly influence the physical properties of materials. On the other hand, the low-energy-scale behavior is often determined by electronic structure changes which occur on a much higher energy scale. Well-known examples are the Kondo systems in which the low-energy-scale properties are caused by high-energy-scale local atomic Coulomb and exchange interactions. Another more simple example is the transition-metal impurity-induced scattering of electrons at the Fermi level which is often caused by impurity potentials with a d resonant energy far removed from the Fermi level. Recently, we have shown[14,15] that ultraviolet photoelectron spectroscopy (UPS) and bremsstrahlung isochromat spectroscopy can provide detailed information concerning the impurity-induced changes in the density of states. Also, an attempt has recently been made to interpret transport properties and UPS data of a number of alloys in a unified approach.[16]

In this paper we present and discuss the UPS spectra of Pd and Pt impurities in noble-metal hosts. We derive from the spectra the impurity-induced changes in the density of states and show that a simple model calculation can explain the data with surprising accuracy. We show that spin-orbit effects are important especially for Pt impurities and also for Au as host. For *Cu*Pd there is a large discrepancy between experiment and first-principles calculations, whereas the simple model works well. We argue that this is due to a neglect of lattice relaxation in the former. We discuss the effects of lattice strain on the local impurity density of states using a model Hamiltonian. A direct extension of the model used permits us to predict changes in the host d-band density of states and UPS spectra resulting from vacancies in the lattice.

II. EXPERIMENTAL PROCEDURE

The UPS spectra of polycrystalline Cu, *Cu*Pd(5 at. %), *Cu*Pt(2 at. %), Ag, *Ag*Pd(3 at. %), *Ag*Pt(2 at. %), Au, *Au*Pd(4.5 at. %), and *Au*Pt(4.5 at. %) were collected with a double-pass cylindrical mirror analyzer[17] (CMA) in an angular integrated mode. The CMA was operated at 10 eV pass energy, giving an overall resolution of the instrument of 85 meV. The base pressure was 1×10^{-10} Torr. No noticeable changes in the spectra were found during the 30-min scans immediately following sample cleaning. The cycles of cleaning and measuring were repeated until about 10^5 counts were accumulated in the most intense channels that were distributed in 37.5-meV intervals over the 10-eV-wide valence-band regions covered in the experiment. Clean surfaces were obtained by means of Ar-ion bombardment. The possibility of compositional changes due to preferential sputtering was checked with core-level x-ray photoelectron spectroscopy (XPS) in a separate vacuum chamber. No such effects could be found in the alloys discussed here. We are quite confident, therefore, that our UPS spectra are representative of the dilute limit.

The light source was a He lamp adjusted such, as to optimize He I radiation. The kinetic energies of the photoemitted electrons lie in the 6—16 eV region, which is an energy range of relatively large escape depths (typically 10—15 Å,[18] compared to the 2—3 Å thickness of the sur-

face layer in noble metals), so that our spectra are dominated by bulk photoemission.

The Cu-based samples were the same as in Ref. 8. The Au- and Ag-based alloys were supplied Dr. A. Myers and co-workers.[19] All samples were obtained from melting the weighted quantities of the components in a sealed quartz tube.

III. RESULTS AND DISCUSSION

In Figs. 1 to 3 the spectra for Pt and Pd in Cu, Ag, and Au are shown, together with the pure noble-metal spectra. These spectra were subsequently corrected for the 23.08-eV He satellite, the intensity of which was 1.7% relative to the 21.22-eV main line as determined from the echo in the Ni Fermi edge. In addition, we applied a $1/E$ correction[20] to the intensity to account for the energy-dependent transmission of our analyzer. Finally, the scattered electron background was subtracted,[21] which is a necessary procedure as we want to integrate the spectral intensities later. For this purpose it was assumed, that the electron-energy-loss spectrum can be represented with a step function. The scattered electron background then corresponds to the integral of the background-free UPS spectrum. The relative weight of the background contribution is determined iteratively by fitting the background intensity in the energy region below the bottom of the bands. As the resulting background contributions are very smooth functions of energy this procedure does not introduce artificial sharp features in the corrected spectra. The resulting spectra are shown in Figs. 4 to 6.

The spectra shown in Figs. 4 to 6 exhibit structure between the host-metal d bands and the Fermi level due to the impurity d states. The clearest examples of cases where the impurity d state is well separated from the host

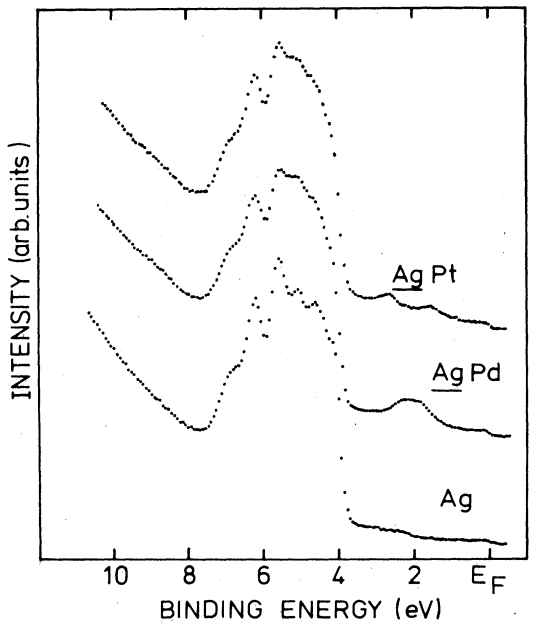

FIG. 2. UPS spectra of *Ag*Pd (3 at. %), *Ag*Pt (2 at. %), and Ag.

d band is *Ag*Pd and *Ag*Pt shown in Fig. 5. In these cases one clearly sees the influence of the spin-orbit coupling. This is most obvious for *Ag*Pt. However, we also notice that the Pt d peak closest to the Fermi level ($d_{5/2}$) is broader. In a previous paper this has been examined in detail,[22] and we have shown that the spectrum can be understood if we take into account a cubic-crystal-field split-

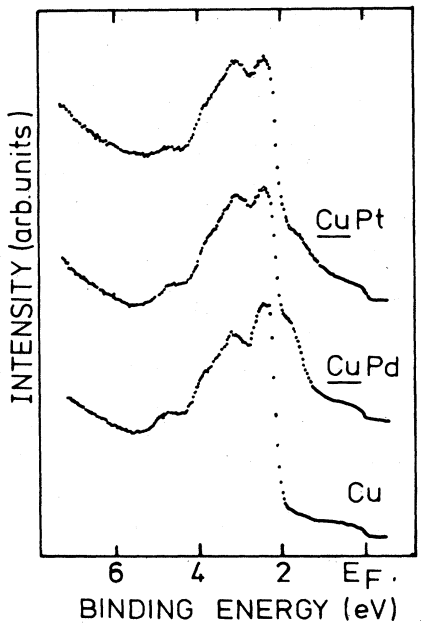

FIG. 1. UPS spectra of *Cu*Pd (5 at. %), *Cu*Pt (2 at. %), and Cu.

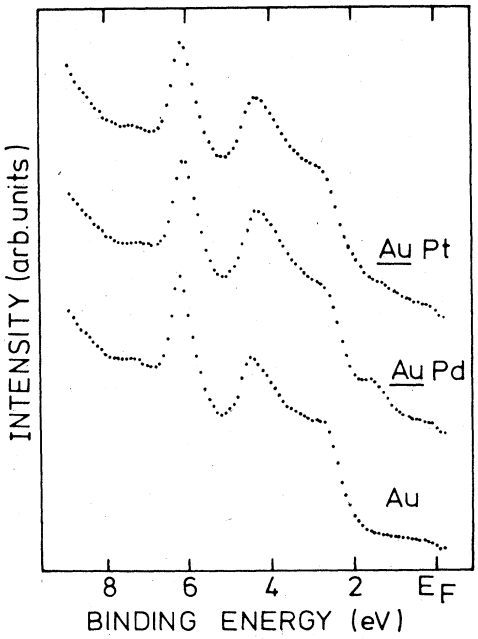

FIG. 3. UPS spectra of *Au*Pd (4.5 at. %), *Au*Pt (4.5 at. %), and Au.

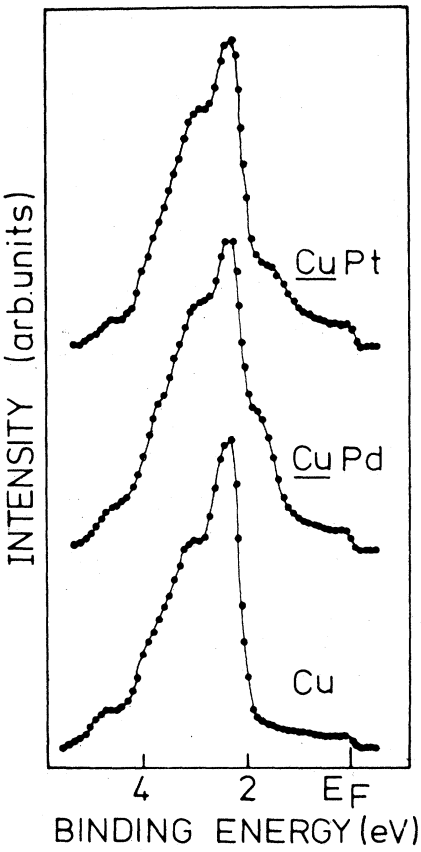

FIG. 4. Corrected UPS spectra for Cu, *Cu*Pd, and *Cu*Pt. The thin solid lines are a guide to the eye.

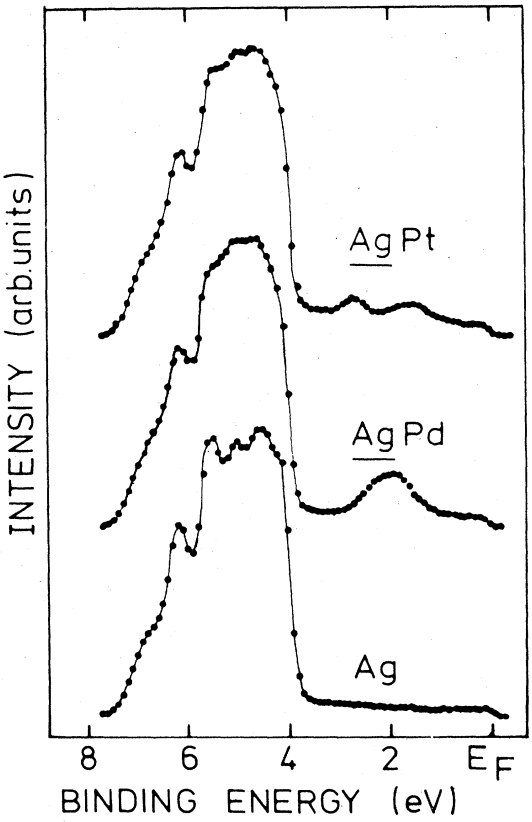

FIG. 5. Corrected UPS spectra of Ag, *Ag*Pd, and *Ag*Pt. The thin solid lines are a guide to the eye.

ting. In the O_h double group the d states span the Γ_7, Γ_8, and $\Gamma_{8'}$ irreducible representations causing (for small crystal field) the $d_{5/2}$ line to split into two components. Also, in *Ag*Pd there is evidence of the spin-orbit coupling of Pd resulting in the shoulder at the high-binding-energy side of the peak as we will see below.

For the Au and Cu hosts the impurity d structure is visible only as shoulders at the top of the host-metal d bands. This is not unexpected since the top of the d band for Au and Cu lies much closer to the Fermi level than in Ag. If, as expected, the Pd and Pt impurity d-state energy is the same for the three noble-metal hosts, the impurity states will be either just in or just outside the Au and Cu host d bands. The virtual-bound-state peak positions and half widths at half maximum are given in Table I and compared to the XPS data of Hüfner, Wertheim, and Wernick.[23] We see from the table that the peak positions agree quite well, but the linewidths are different, probably due to the better resolution in our measurements. A similar agreement exists with the XPS data on *Cu*Pd of

TABLE I. Experimental UPS impurity peak maxima (ϵ_{max}) and half widths at half maximum (Γ): (a) this work and (b) taken from Ref. 23. Parameters that were used in the theoretical spectra: change in impurity d potential (Δ), s-d coupling (σ_s), spin-orbit coupling (ξ_d), cubic crystal field (D_q), and average energy position of the impurity d states $\bar{\epsilon}_d+\Delta$, where $\bar{\epsilon}_d$ is the average host d-band energy.

Solid	(a) ϵ_{max} (eV)	(a) Γ (eV)	(b) ϵ_{max} (eV)	(b) Γ (eV)	Δ (eV)	Imσ_s (eV)	ξ_d (eV)	D_q (eV)	$\bar{\epsilon}_d+\Delta$ (eV)
Cu					0	0	0	0	−3.52
*Cu*Pd	1.8	0.30±0.07	1.75	0.28	1.0	0.30±0.07	0.12	0	−2.52
*Cu*Pt	1.65/2.0	0.35±0.07			1.18	0.35±0.07	0.31	0	−2.34
Ag					0	0	0	0	−5.68
*Ag*Pd	1.8/2.2	0.40±0.05	1.95	0.35	3.4	0.40±0.05	0.18	0	−2.28
*Ag*Pt	1.5/2.6	0.28±0.07	1.95	0.47	3.23	0.28±0.07	0.44	0.043	−2.45
Au					0	0	0.45	0	−5.02
*Au*Pd	1.6	0.40±0.10	1.55	0.18	2.1	0.40±0.10	0.18	0	−2.92
*Au*Pt	1.3/1.9	0.50±0.10			2.1	0.50±0.10	0.44	0	−2.92

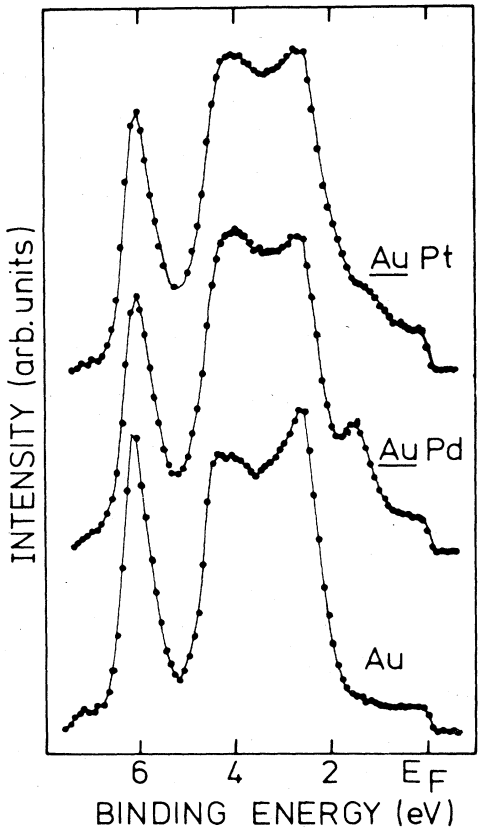

FIG. 6. Corrected UPS spectra of Au, *Au*Pd, and *Au*Pt. The thin solid lines are a guide to the eye.

Mårtensson *et al.*[24] General agreement exists with recent angle-resolved UPS (ARUPS) investigations on Cu-Pd random alloys (Refs. 25 and 26), older UPS (Ref. 27), and XPS (Ref. 28) work on *Cu*Pd, UPS (Ref. 29), and XPS (Ref. 30) work on *Cu*Pt and UPS work on *Ag*Pd (Refs. 21 and 31).

In addition to this extra structure we also notice changes in the host *d*-band density of states. This is most obvious for the Ag alloys where we see a partial smearing of the sharp features in the density of states. To demonstrate this more clearly we show in Figs. 7 to 9 the difference spectra. To obtain these, we first normalized the experimental curves integrated up to the Fermi level. The difference spectra clearly show substantial changes in the host-metal *d*-band density of states upon alloying, in addition to the extra structure discussed above. Sharp structure in the difference spectra occur at energies where the host *d*-band structure shows a strong variation with energy in the density of states. We also notice that the difference spectra are rather independent of the type of impurity involved and are primarily negative in the host *d*-band region, as they should be since the impurity substitution must move *d* density out of the host *d* band to build up the impurity *d* states just outside of the host band.

To explain these features we resort to a simple model Hamiltonian discussed in our treatment of Mn impurities in Ag and Cu.[15] The model Hamiltonian is based on two basic assumptions: first, that a one-particle Hamiltonian

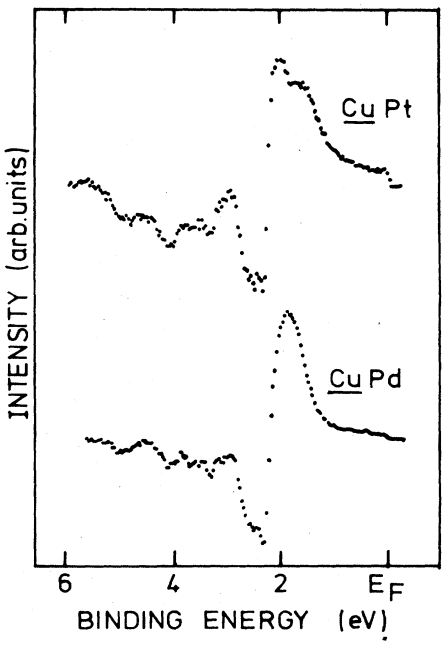

FIG. 7. Difference UPS spectra: *Cu*Pd-Cu and *Cu*Pt-Cu.

can be used in the description of photoemission of the systems studies, and second, that the impurity *d* electrons couple with the host-metal states with matrix elements equal to those determining the host-metal band structure. The only difference then, in the Hamiltonian describing the impurity system, is that the impurity *d* states are shifted in energy relative to those of the host. This is

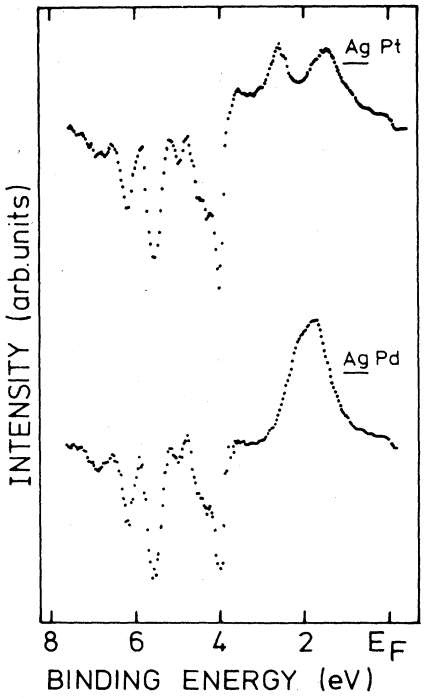

FIG. 8. Difference UPS spectra: *Ag*Pd-Ag and *Ag*Pt-Ag.

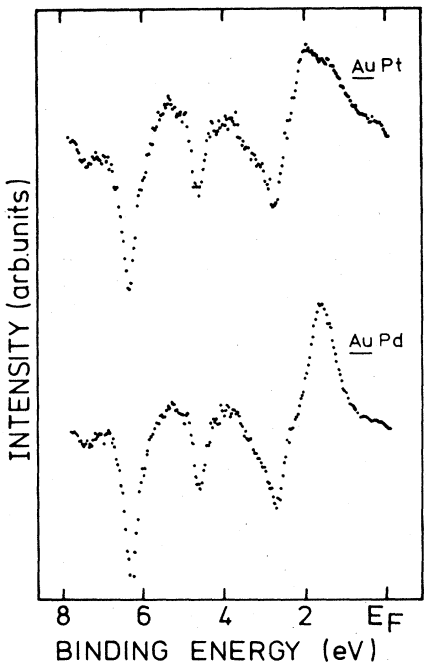

FIG. 9. Difference UPS spectra: *Au*Pd-Au and *Au*Pt-Au.

often referred to as the Clogston-Wolff model.

Before describing the theoretical results we make a few remarks concerning the validity of the above assumptions for the systems of interest. The *d*-*d* Coulomb and exchange interactions are known to be quite large for Pd (Ref. 32) and are expected to be only slightly smaller for Pt. At first glance one might then expect corelation effects to be important, especially in view of the rather narrow impurity states observed. However, we also find that the peak in the impurity density of states is well below the Fermi level, so that any impurity *d* holes present in the ground state are distributed in a large energy range above the Fermi level, in the sense of Hartree-Fock theory. We also know that correlation effects in the UPS spectra are only important if there are other *d* holes present with which the created *d* hole can correlate and if the *d* holes present are distributed over an energy range small or comparable to the *d*-*d* Coulomb interactions. We therefore expect correlation effects to be important in UPS only if the *d* holes present in the ground state are also confined to a narrow energy range as, for example, in Ni metal.[33] We expect Pd and Pt impurities to behave in a similar manner to Cu and Ag as far as UPS is concerned. In the latter there are also *d* holes present in the ground state, but they occur in a broad *sp*-like band due to hybridization. This is the reason for the success of one-particle theory for describing the UPS spectra of Cu. Of course, if, as in Auger spectroscopy, two *d* holes are created in the narrow *d* band or *d* impurity state region, the correlation effects may, and in fact do, dominate the spectral distribution.[34] To summarize: As long as we confine ourselves to the $(N-1)$-electron density of states (UPS), correlation effects for the systems studied can be neglected.

The second approximation is more difficult to justify for all the systems studied. To discuss it we resort to a tight-binding description of the host-metal *d* band:

$$H_d=\sum_{i,j} T_{ij} d_i^{\dagger} d_j \tag{1}$$

with

$$T_{ij}=\langle \Psi_{d_i}^{\text{host}} | H | \Psi_{d_j}^{\text{host}} \rangle$$

and i and j labeling the lattice sites. We neglect the orbital degeneracy here since it is not important for this discussion. The assumption then is that for an impurity at site $i=0$,

$$\langle \Psi_{d_0}^{\text{imp}} | H | \Psi_{d_j}^{\text{host}} \rangle = \langle \Psi_{d_0}^{\text{host}} | H | \Psi_{d_j}^{\text{host}} \rangle \ , \tag{2}$$

which implies that if the interatomic distances are equal then, also, the *d* wave functions must have the same radial extent. We expect this to be a good approximation for *Ag*Pd, *Au*Pt, and *Cu*Ni; however, for systems like *Cu*Pt or *Cu*Pd one might expect the above approximation to be invalid especially if the Pt and Pd-Cu interatomic distances were equal to the Cu-Cu distances.

However, we certainly expect the lattice to relax upon the introduction of a large atom like Pd into Cu. In fact, one expects the Pd-Cu nearest-neighbor distances to be closer to the sum of the Pd and Cu metallic atom radii than 2 times the Cu atomic radii. Such a lattice distortion has the tendency towards the result assumed as given by Eq. (2). It is interesting to note that the near equality of the total *d*-band widths in pure Cu and Ag suggests that the lattice parameters adjust in such a way as to keep the nearest-neighbor *d*-*d* transfer integrals constant.

In a recent discussion of UPS spectra of Mn impurities in noble metals[15] we derived the following expressions for the total difference and local impurity density of states for a Clogston-Wolff model Hamiltonian:

$$\Delta\rho=-\pi^{-1}\text{Im}\left[\frac{(\Delta+\sigma_s)(\partial/\partial\epsilon)g_0^0(\epsilon)}{1-(\Delta+\sigma_s)g_0^0(\epsilon)}\right] , \tag{3}$$

$$\rho_{\text{loc}}=\pi^{-1}\text{Im}\left[\frac{g_0^0}{1-(\Delta+\sigma_s)g_0^0(\epsilon)}\right] , \tag{4}$$

where $\Delta=\epsilon_d^i-\bar{\epsilon}_d$ is the impurity *d*-state energy relative to the host *d*-band centroid, σ_s is the imaginary optical potential describing the mixing of the impurity *d* state with the host *sp* bands, and g_0^0 is the *d*-projected Green's function of the pure host metal. We also showed that the energy-dependent optical matrix elements in UPS can be included by simply replacing the Green's function in the numerator of Eq. (3) by that obtained from the UPS spectrum of the pure material:

$$\Delta\rho=-\pi^{-1}\text{Im}\left[\frac{(\Delta+\sigma_s)(\partial/\partial\epsilon)g_{\text{expt}}(\epsilon)}{1-(\Delta+\sigma_s)g_0^0(\epsilon)}\right] . \tag{5}$$

In these expressions we have not taken account of spin-orbit and crystal-field effects. A full calculation taking these effects into account and also deviations from the Clogston-Wolff model are presented in the Appendix.

For the systems of interest here a suitable basis set of states to use is that determined by the irreducible repre-

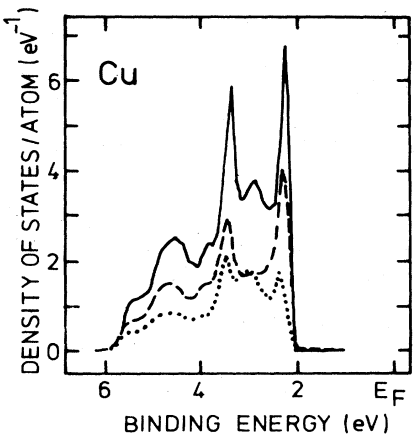

FIG. 10. Density of states of copper. Solid line: Total d density of states. Dashed line: t_{2g} projected DOS. Dotted line: e_g projected DOS.

sentations, spanned by a d state, of the cubic double point group. These are $\Gamma_8(e_g)$, $\Gamma_8(t_{2g})$, and $\Gamma_7(t_{2g})$. In the Appendix we have derived general expressions for the change in the total density of states and impurity local density of states given by Eqs. (A42) and (A43). In these expressions we require knowledge of $(\Delta+\sigma_s)^{\nu}_{\mu}$, now in matrix form, and the local Green's function corresponding to the pure host $g^{0\nu}_{0\mu}(\epsilon)$. These equations are in general quite cumbersome to work with because of the occurrence of two, in general, nondegenerate Γ_8 representations, so that diagonalization of $g^{0\nu}_{0\mu}(\epsilon)$ requires an energy-dependent transformation matrix. However, a very simple form results if we can neglect the difference in $g^{0t_{2g}}_{0t_{2g}}$ and $g^{0e_g}_{0e_g}$. In this case we can rotate the basis set and use instead $\Gamma_7(d_{5/2})$, $\Gamma_8(d_{5/2})$, and $\Gamma_8(d_{3/2})$ on which g^0_0 is diagonal:

$$g^{\Gamma_7(d_{5/2})}_{\Gamma_7(d_{5/2})}=g^{\Gamma_8(d_{5/2})}_{\Gamma_8(d_{5/2})}=g^{5/2}_{5/2}\ ,$$

$$g^{\Gamma_8(d_{3/2})}_{\Gamma_8(d_{3/2})}=g^{d_{3/2}}_{d_{3/2}}\ .$$

To demonstrate the validity of these in Fig. 10 we show the Cu t_{2g} and e_g projected and total d density of states. We see that there is little difference in these and even their mean energies are equal, justifying the neglect of the cubic symmetry in determining the local host density of states. For Cu and Ag the spin-orbit coupling is also negligible in g^0_0, so that $g^{d_{3/2}}_{d_{3/2}}=g^{d_{5/2}}_{d_{5/2}}$. For Au, however, we will find spin-orbit coupling to be quite important.

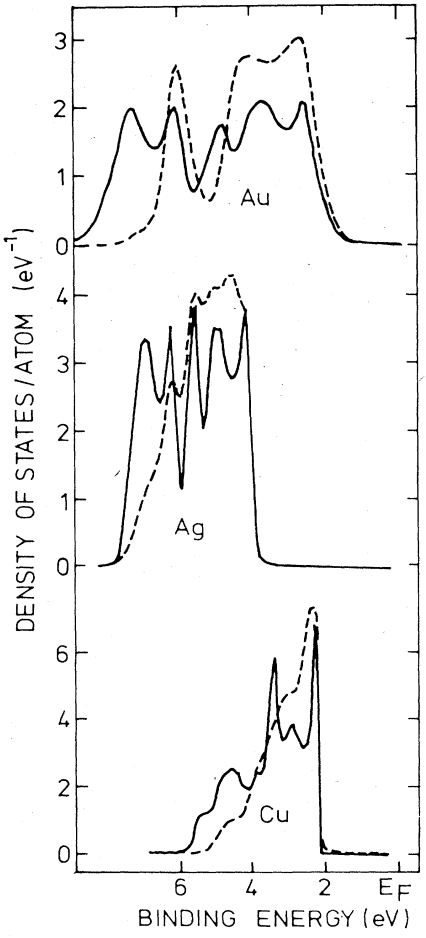

FIG. 11. Imaginary parts of theoretical (solid lines) and experimental (dashed lines) Green's functions of Cu, Ag, and Au.

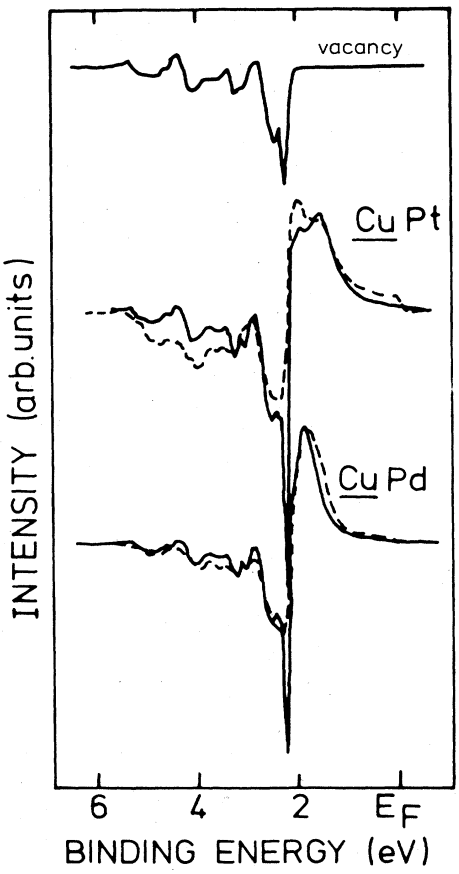

FIG. 12. Theoretical (solid lines) and experimental (dashed lines) UPS difference spectra of a vacancy in Cu, *Cu*Pt-Cu, and *Cu*Pd-Cu.

In terms of the above basis the matrix elements of $\Delta+\sigma_s$ are given by

$$\begin{aligned}
&\langle\Gamma_7(d_{5/2})|(\Delta+\sigma_s)|\Gamma_7(d_{5/2})\rangle=\Delta+\delta\xi_d-4Dq+\sigma_s\ ,\\
&\langle\Gamma_8(d_{5/2})|(\Delta+\sigma_s)|\Gamma_8(d_{5/2})\rangle=\Delta+\delta\xi_d+2Dq+\sigma_s\ ,\\
&\langle\Gamma_8(d_{3/2})|(\Delta+\sigma_s)|\Gamma_8(d_{3/2})\rangle=\Delta-\tfrac{3}{2}\delta\xi_d+\sigma_s\ ,\\
&\langle\Gamma_8(d_{5/2})|(\Delta+\sigma_s)|\Gamma_8(d_{3/2})\rangle=-2\sqrt{6}Dq\ ,
\end{aligned}\tag{6}$$

where $\delta\xi_d$ is the difference in spin-orbit coupling between impurity and host, Δ is the average impurity d energy relative to the centroid of the host d band, $10Dq$ is the crystal-field splitting of the impurity, and σ_s describes the coupling to the host sp band. All of these quantities are treated as parameters which determine the position (Δ), widths (σ_s), and splitting ($\xi_\delta, 10D_q$) of the impurity d states appearing outside of the host d bands. To get the total impurity-induced change in the density of states using Eq. (A43) and (A44) we further require knowledge of the pure host-metal local d Green's function which determines D and the experimental host d Green's function appearing in Eq. (A44). These were obtained from the interpolation calculation of Smith and co-workers[35] and the experimental pure host measurements shown in Fig. 11. The smooth "sp" parts of the DOS were subtracted from both the theoretical and experimental data resulting in the d bands of finite width shown in Fig. 11 for Cu, Ag, and Au. A Hilbert transform of the so-obtained density of states provided the real part of the host local d Green's functions.

In Figs. 12–14 we show the calculated difference UPS spectra using Eq. (A44) and the parameters given in Table I, together with the experimental difference spectra. The agreement between theory and experiment is surprisingly good. The theory predicts all the structures seen in the host d band regions in addition to the impurity states outside the host d band. There are differences in the relative amplitudes and widths, but we consider these as minor in view of the simple model used as well as the background subtraction techniques used in the experimental data.

The structure in the host-metal d-band region is primarily the result of changes in the band structure due to the removal of a noble-metal atom.[36] This reduces the number of bonds of the neighboring atoms, thereby reducing their bandwidths. A similar band-narrowing effect occurs at the surface also, because of a decrease in the coordination number. To demonstrate that this is the dominant contribution we also show in Figs. 12–14 the calculated difference spectrum for a vacancy. This calculation was done by taking $\Delta\rightarrow\infty$ in Eq. (A44) so that

$$\Delta\rho=\pi^{-1}\mathrm{Im}\left[g_0^0(\epsilon)^{-1}\frac{\partial}{\partial\epsilon}g_{\mathrm{expt}}(\epsilon)\right]\ .\tag{7}$$

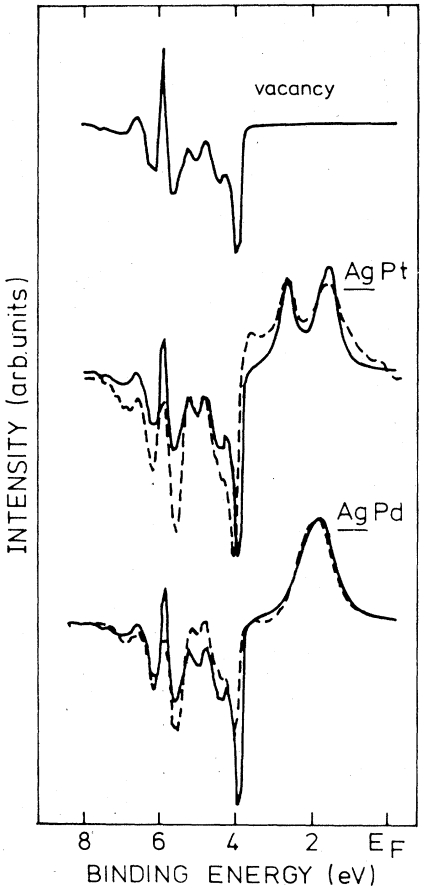

FIG. 13. Theoretical (solid lines) and experimental (dashed lines) UPS difference spectra of a vacancy in Ag, *Ag*Pt-Ag, and *Ag*Pd-Ag.

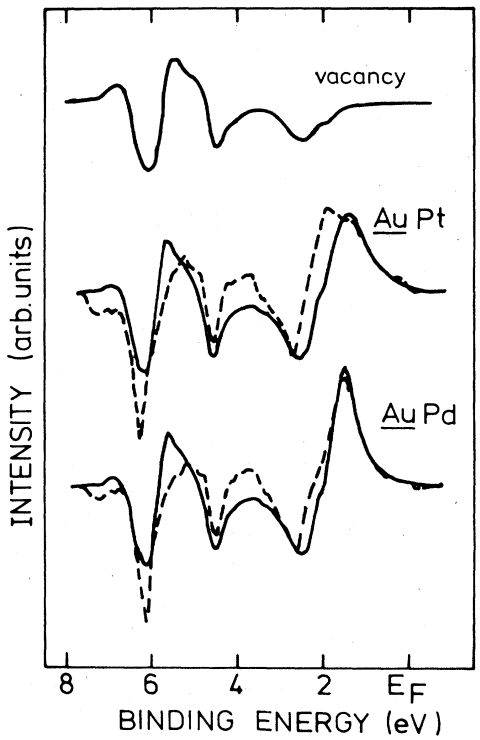

FIG. 14. Theoretical (solid lines) and experimental (dashed lines) UPS difference spectra of a vacancy in Au, *Au*Pt-Au, and *Au*Pd-Au.

We see the same structures occurring in the *d*-band region as for the Pd and Pt impurities although their amplitudes are slightly different.

The amplitudes of the oscillations in the vacancy difference spectra are expected to be proportional to the vacancy density. It would therefore be quite interesting to study purposely damaged materials. Note that experimental details, such as resolution, photon energy (in any range), and geometry of the setup are all effectively taken into account in Eq. (7).

To demonstrate the influence of the optical matrix elements as included in Eq. (A44) we also calculated the to-

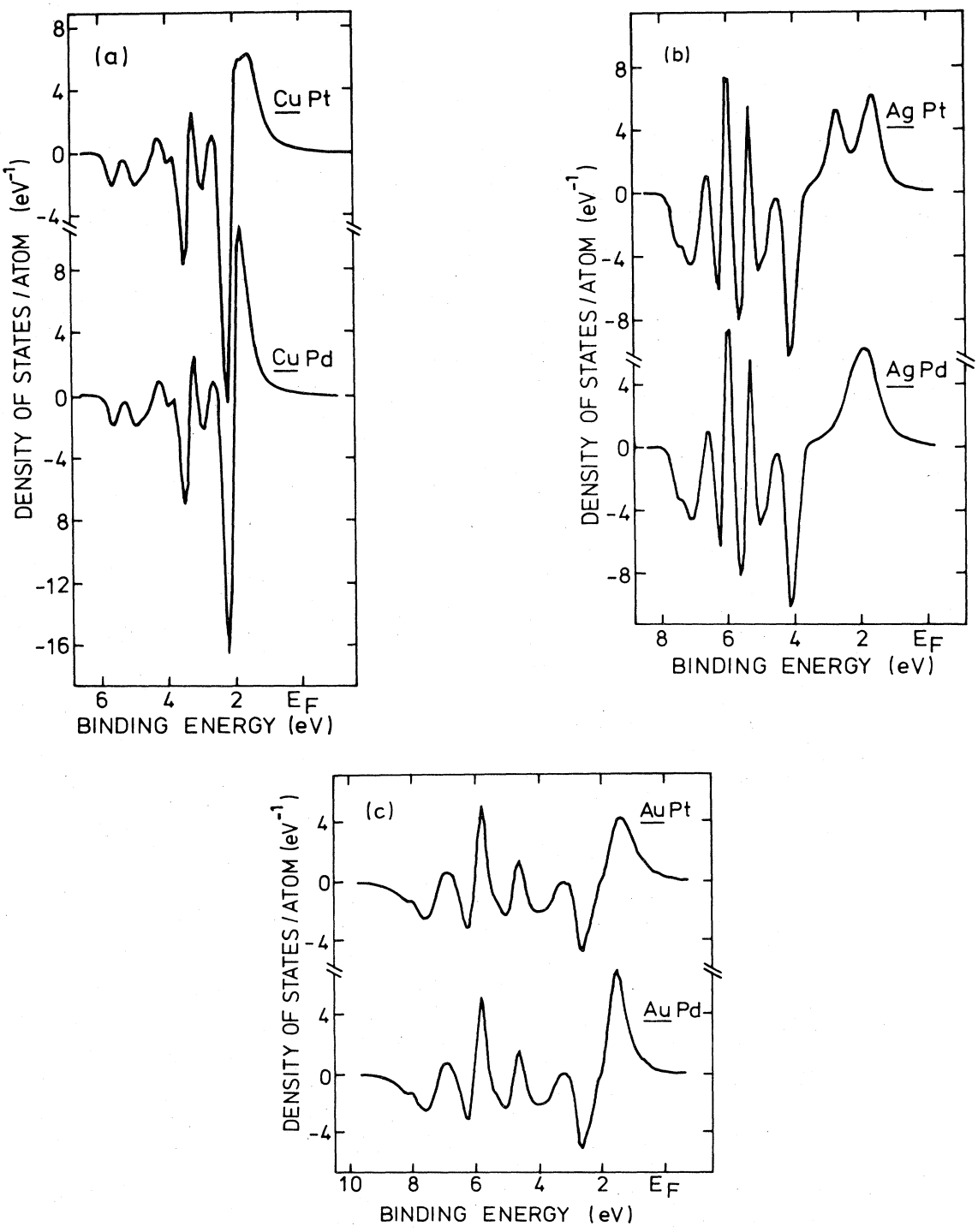

FIG. 15. Theoretical difference densities of states of (a) *Cu*Pt-Cu and *Cu*Pd-Cu, (b) *Ag*Pt-Ag and *Ag*Pd-Ag, and (c) *Au*Pt-Au and *Au*Pd-Au.

tal difference density of states using Eq. (A43). These are shown in Fig. 15. Comparison of these to the calculated difference UPS spectra clearly shows that matrix-element effects must be included in comparing experiment to theory.

We are now in a position to calculate the local impurity density of states using the parameters of Table I and Eq. (A42). These are shown in Fig. 16. We clearly see the spin-orbit splitting of the Pt virtual bound states in *Ag*Pt. This is less visible in *Cu*Pt and *Au*Pt because here the primarily $d_{3/2}$ state lies inside the host d band and the $d_{5/2}$ state just outside. The $d_{3/2}$ state therefore is delocalized because of its strong mixing with the host d band while the $d_{5/2}$ state remains quite localized. Also, for the Pd impurities the spin-orbit coupling is quite important, contributing strongly to the total width of Pd virtual bound state in *Ag*Pd. Rather interesting is the narrowing of the virtual bound state on going to Cu and Au hosts. This is due to the fact that here the $d_{3/2}$ is just inside the host d band and $d_{5/2}$ is just outside. We also notice the large amount of impurity d character in the host band for Cu and Au due to the d-d hybridization. This makes the often used Lorentzian line-shape assumption of the impurity state incorrect.

The large coupling of the impurity d state with the host d band causes the impurity d character to delocalize. Also, for the same reason some host-metal d character is localized at energies corresponding to the impurity virtual-bound-state position. We can get a better idea of this delocalization by comparing the local impurity density of states to the change in the total density of states. In Table II we list the amount of impurity character so obtained in the states at the virtual-bound-state peak and at the Fermi level. We see that at the virtual-bound-state peak energy there is a considerable amount of host d character ranging up to 35% for *Cu*Pd. Although the change in density of states at the Fermi level is mostly of impurity d character here also, as much as 15% (*Ag*Pt) is of host-metal d character. It is also interesting to determine the character of the total displaced charge. This can be

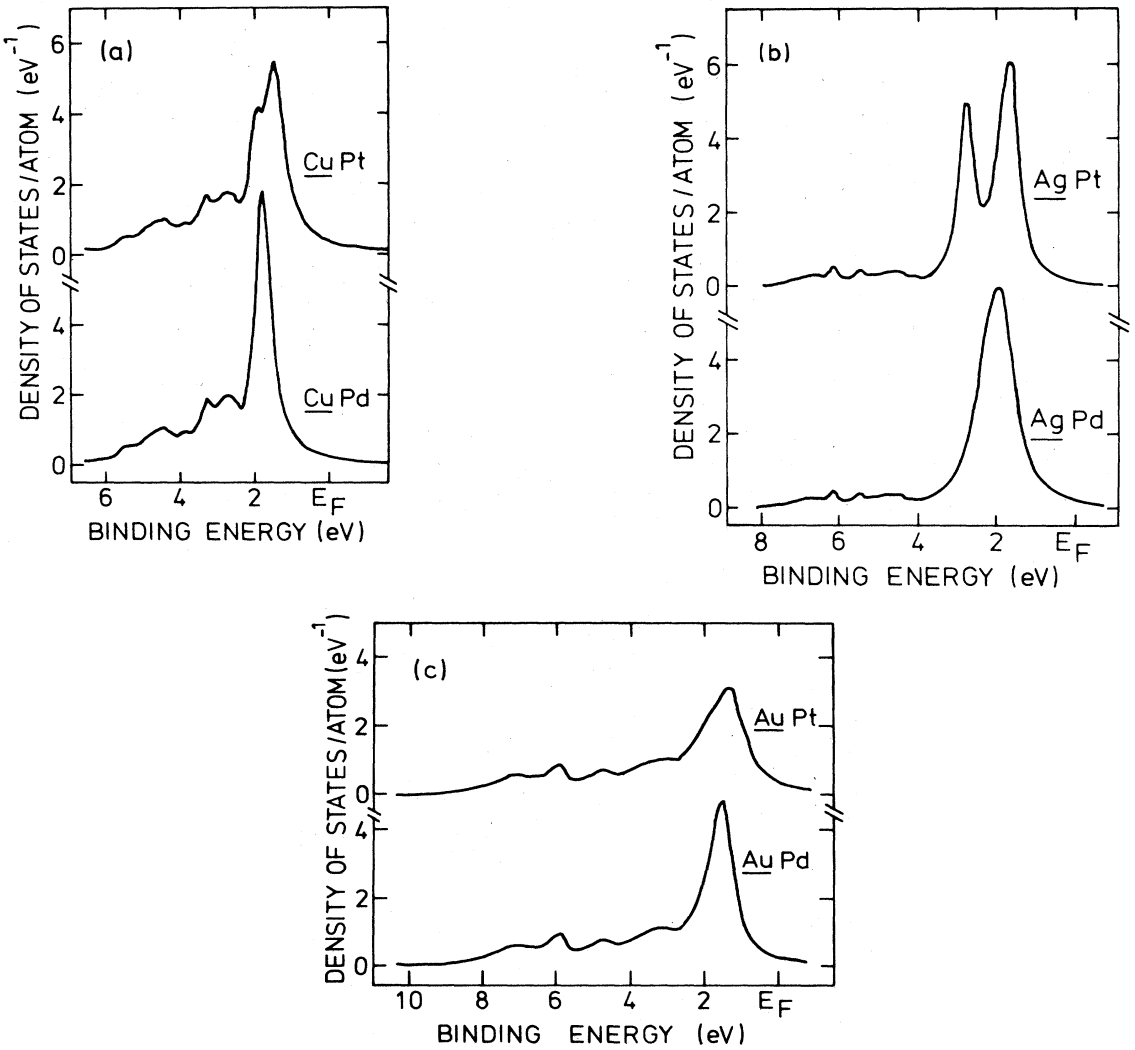

FIG. 16. Local d projected DOS at a Pd and Pt site in (a) a copper host, (b) a silver host, and (c) a gold host.

TABLE II. Relative amount of impurity d character in the virtual bound state at peak maximum, at E_F and in the displaced d charge. This is the quotient of the local DOS and difference DOS (first two columns) and of the integrated unoccupied local DOS and difference DOS (third column).

Solid	$I(E_{max})$	$I(E_F)$	I(DOS above E_F)
*Cu*Pd	65%	98%	98%
*Cu*Pt	75%	98%	98%
*Ag*Pd	93%	98%	99%
*Ag*Pt	87%	99%	99%
*Au*Pd	69%	87%	94%
*Au*Pt	76%	86%	95%

obtained by integrating the local impurity DOS and the change in the total density of states from the Fermi level to infinity. We see from Table II that the total displaced charge is again mainly of impurity character although up to 5% is located on host atoms for the Au-based alloys. This implies that it is still a reasonable approximation to relate the impurity-induced scattering to the local displaced charge, although it is conceptually better to think in terms of the total displaced charge. This should obey the Friedel sum rule exactly.

Of interest for the interpretation of transport measurements are the d scattering phase shifts at E_F. In the Appendix we show their relationship to the total displaced d charge [Eqs. (A49) and (A50)]. These are listed in Table III together with the total change in the d density of states at the Fermi level. For comparison we also listed some experimentally determined phase shifts.[22,37–39]

IV. LATTICE RELAXATION

At first glance it is rather surprising that a Clogston-Wolff-like model does so well. As mentioned above, we expect it to be valid for *Ag*Pd and *Au*Pt, but the agreement with experiment for *Cu*Pd, *Cu*Pt, and *Ag*Pt is somewhat surprising. This is because one might have expected the Pd-Cu d-d overlap to be considerably different from the Cu-Cu d-d overlap. In this context it is interesting to compare our local density of states to that obtained from first-principles calculations[5] shown in Fig. 17. We notice a large difference between the two calculations especially in the Cu d-band region. The most obvious difference is seen at the bottom of the Cu d band where the first-principles calculation shows a substantial peaking, whereas our model calculation shows a small impurity contribution. The same peaking can also be seen in the CPA calculation of Rao *et al.*[25] and in the self-consistent Korringa-Kohn-Rostoker—coherent-potential-approximation (KKR-CPA) calculation of Stocks and coworkers.[40,41] In a recent analysis of Pd Auger spectra Davies and Weightman[42] showed that agreement with recently published impurity Auger theory[43,44] could only be obtained if the above-mentioned peaking in the impurity local density of states was removed. Also, our UPS data is in much better agreement with our model calculation. The UPS data of Rao *et al.*[25] show indeed a small extra feature at the bottom of the d band, but the intensity is much lower than that predicted by their CPA calculation. Also the valence-band XPS data[23,24] do not reveal the extra DOS at ~6-eV binding energy.

We conclude from all this that the first-principles calculations strongly overestimate the Pd impurity density of states at the bottom of the Cu band. The reason for this probably is that the calculations were done for an unrelaxed lattice. In our calculation we essentially assume that the lattice relaxes in such a way as to make the Pd-Cu d-d overlap equal to that of Cu-Cu. This is similar (but not equivalent) to saying that the lattice relaxes in such a way as to keep the interatomic distance equal to the sum of the atomic radii. In the first-principles calculation we then expect the Cu-Pd d-d overlap to be strongly overestimated if the lattice is kept unrelaxed. It is interesting to see what we would get in this case. In the Appendix we calculated the impurity density of states for a tight-binding model including a possible difference between the impurity-host and host-host d-d transfer integral. We show there that

$$\rho_{\text{imp}}=\pi^{-1}\text{Im}\left[\frac{g_{d0}^{d0}}{(1+t)^2-\{[(1+t)^2-1](E-\bar{E}_d)+\Delta+\sigma_s\}g_{d0}^{d0}}\right], \tag{8}$$

TABLE III. Changes in d density of states at E_F [$\Delta n_d(E_F)$] and $l=2$ scattering phase shifts [$\pi^{-1}\eta_d(E_F)$] compared to experimental phase shifts.

Solid	$\Delta n_d(E_F)$ (eV^{-1})	$\pi^{-1}\eta_d(E_F)$	$\pi^{-1}\eta_d(E_F)$
*Cu*Pt	0.32±0.06	−0.059±0.012	−0.027↔−0.073[a]
*Cu*Pd	0.21±0.06	−0.046±0.012	−0.013↔−0.055[a]
*Ag*Pt	0.23±0.05	−0.038±0.010	−0.032↔−0.042[b]
*Ag*Pd	0.31±0.04	−0.062±0.008	−0.036↔−0.041[c]
*Au*Pt	0.47±0.06	−0.079±0.015	
*Au*Pd	0.35±0.06	−0.063±0.015	−0.053↔0.030[d]

[a]Reference 16.
[b]Reference 22.
[c]References 38 and 39.
[d]Reference 37.

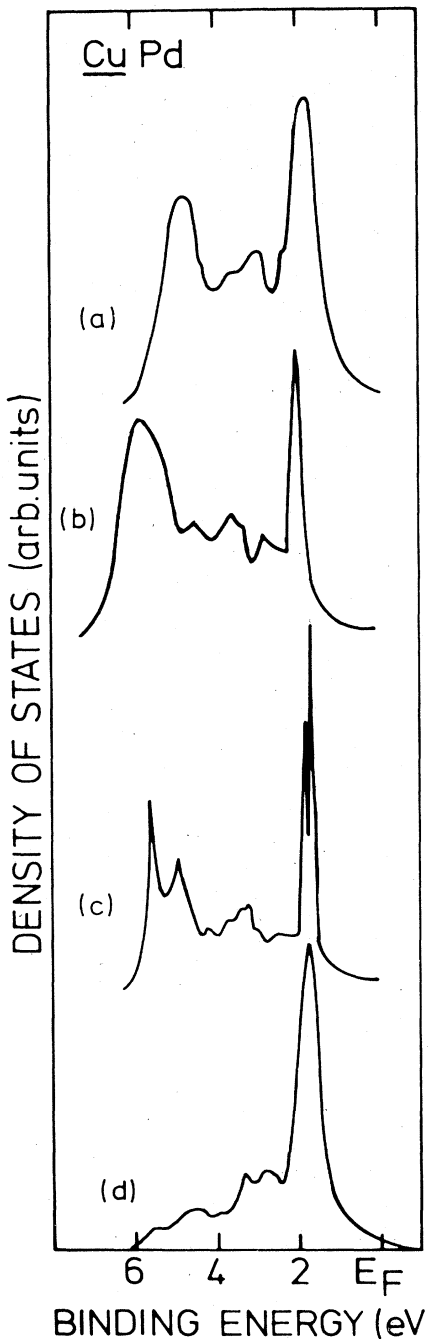

FIG. 17. Local DOS at a Pd site in copper: (a) Ref. 25, (b) Ref. 41, (c) Ref. 5, and (d) this work.

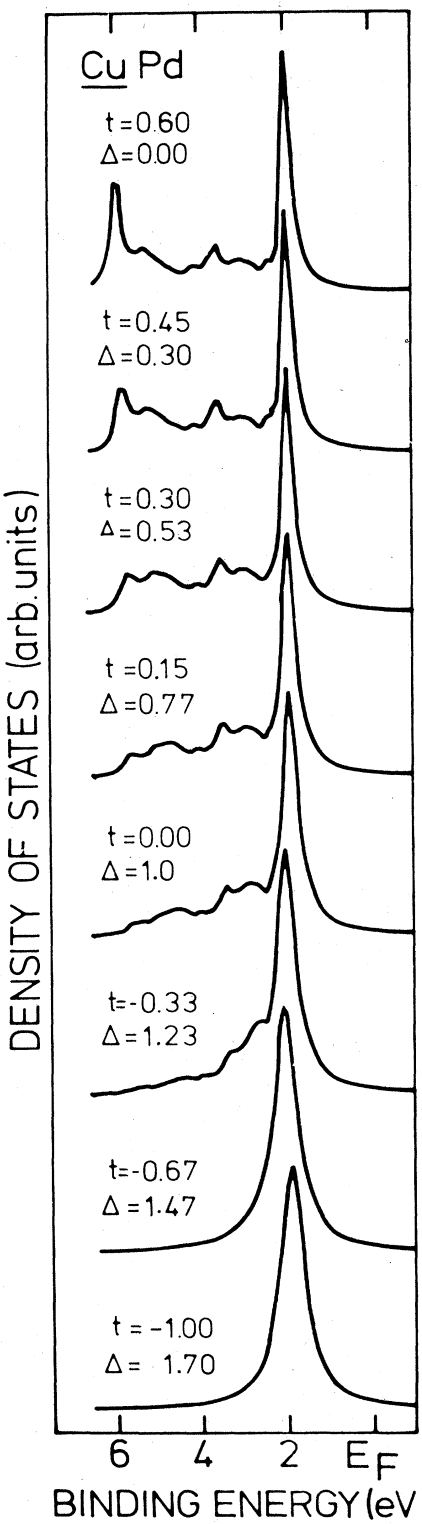

FIG. 18. Local d DOS at a Pd site in *Cu*Pd for some parameter values of the Pd-d—Cu-d transfer matrix element.

where $t=(T_{\text{imp}}^{\text{host}}-T_{\text{host}}^{\text{host}})/T_{\text{host}}^{\text{host}}$.

$\overline{E}_d$ is the centroid of the host d band and the other quantities are the same as in the Clogston-Wolff model. We note that for $t=0$ we are back to the Clogston-Wolff model discussed above. For $t=-1$ the impurity is decoupled from the host d band ($T_{\text{imp}}^{\text{host}}=0$) and we get a Lorentzian virtual bound state only. In Fig. 18 we show the calculated local impurity density of states for various values of t using the Cu host d-band Green's function in Eq. (8). In the calculation Δ was varied in such a way as to keep the virtual-bound-state position constant. We see the enhancement of the impurity density of states at the bottom of the host d band for $t>0$ as compared to $t=0$.

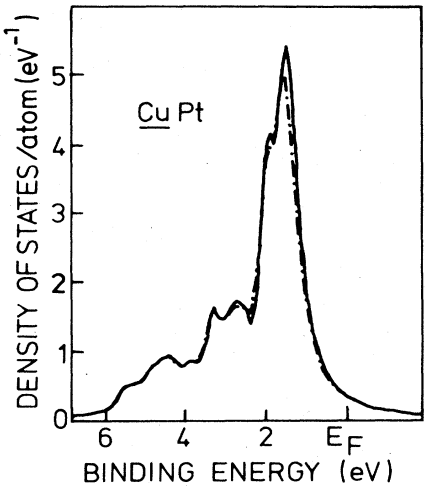

FIG. 19. Local d DOS at a Pt site in CuPt using degenerate (dashed-dotted line) and nondegenerate (solid line) theory.

In fact, for $t \approx 0.6$ we get results close to those obtained from first-principles calculations and this corresponds to $T_{Pd}^{Cu} = 1.6 T_{Cu}^{Cu}$. Indeed, we expect T_{Pd}^{Cu} to be overestimated in the unrelaxed lattice first-principles calculation because of the large size of the Pd atom.

V. DEGENERACY OF THE d BANDS

In order to give an idea of the relevance of taking into account the details of the degeneracy in the d bands, we calculate the local density of states at a Pt site in CuPt again, now using the e_g and t_{2g} projected DOS's (Ref. 45) shown in Fig. 10. The centroids of the e_g and t_{2g} projected DOS's exactly coincide, which means that the average "crystal"-field splitting of the bands is zero. We applied Eq. (A42) of the Appendix to the Green's functions corresponding to these DOS's using the parameter values of Table I for CuPt. In Fig. 19 we compare the so-obtained local density of states of CuPt to the nondegenerate theory of Fig. 15(a). We see that both curves coincide almost everywhere, and we conclude that incorporation of $e_g - t_{2g}$ degeneracy is not relevant here.

A different situation, however, occurs for the Au-based alloys because of the large Au spin-orbit coupling. If, as indicated above, we can neglect the crystal-field effects, we require only the $d_{3/2}$ and $d_{5/2}$ projected density of states to use the equations in the Appendix. In Fig. 20 these projections are shown.[46] The centroids of $d_{3/2}$ and $d_{5/2}$ are at 5.72 and 4.59 eV corresponding to a spin-orbit-coupling parameter of 0.45 eV. Applying Eq. (A42) and Eqs. (6) for the $\Delta + \sigma_s$ matrix components, we obtain the projected and total impurity local density of states as shown in Figs. 21 and 22 for AuPt and AuPd. In these

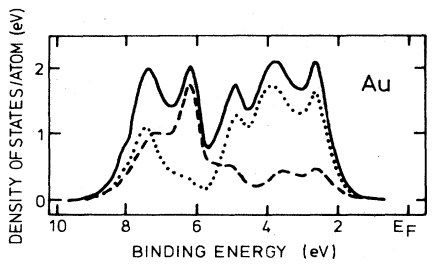

FIG. 20. Density of states of gold. Solid lines: total d density of states. Dashed line: $d_{3/2}$ projected DOS. Dotted line: $d_{5/2}$ projected DOS.

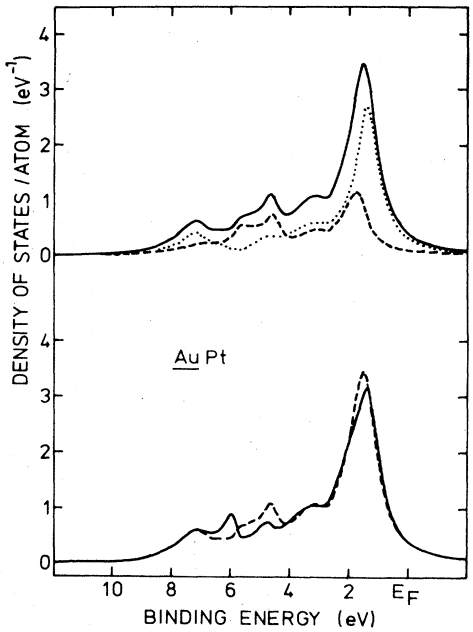

FIG. 21. Local d DOS at a Pt site in AuPt. Upper panel: solid line, total d DOS; dashed line, $d_{3/2}$ projected DOS; dotted line, $d_{5/2}$-projected DOS. Lower panel: solid line, d DOS using nondegenerate theory; dashed line, d DOS using degenerate theory.

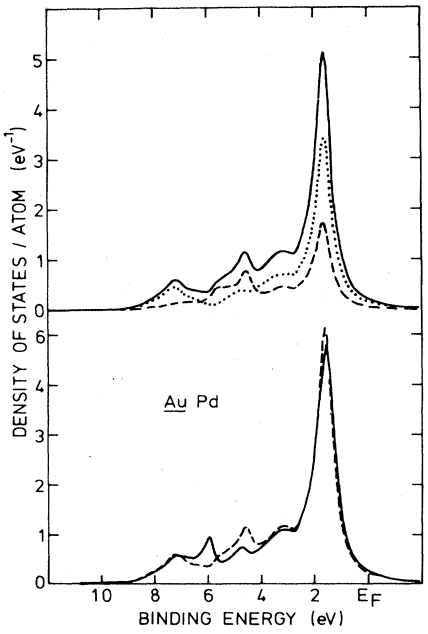

FIG. 22. Local d DOS at a Pd site in AuPd. Dashed and dotted lines: same as in Fig. 21.

figures we also make a comparison with the calculation neglecting the host spin-orbit coupling. We see substantial differences in the host d-band regions and also a small change (7—8%) in the density of d states at the Fermi level. This shows that for Au-based alloys the host spin-orbit coupling should be taken into account.

VI. CALCULATIONS

We have presented high-resolution UPS data for dilute alloys of Pd and Pt in noble-metal hosts. We have obtained the impurity-induced changes in the spectra using difference techniques. We have related the UPS data to scattering properties using a modified version of the Clogston-Wolff and Riedinger approaches, including degeneracy of the d states in the cubic group, spin-orbit splitting, and coupling to the host sp and d bands. We have presented expressions for the difference density of states, the local density of states, and the difference UPS spectra including optical matrix-element effects. We showed that there is good agreement between this theory and experiment allowing us to obtain the bare impurity state energies, the spin-orbit and crystal-field parameters, the virtual-bound-state broadening due to the mixing with the sp band, and the influence of the impurity-d—host-d hybridization. The calculated impurity local density of states using the obtained parameters shows a large mixing with the host d bands. From this we obtained the change in the d density of states at the Fermi level and the related $l=2$ phase shifts which compare favorably with transport measurement. We also discussed the effect of lattice relaxation and demonstrated that the neglect of this can lead to qualitatively incorrect predictions of the local density of states.

ACKNOWLEDGMENTS

We thank M. Vos and C. Westra for checking the surface compositions with XPS. This investigation was supported by the Netherlands Foundation for Chemical Research (SON) with financial aid from the Netherlands Organization for the Advancement of Pure Research (ZWO).

APPENDIX

1. The general form of the transition matrix

To describe the photoelectron spectra and relate them to scattering properties of the impurities, we use a model Hamiltonian that bears some resemblance to the Riedinger approach,[12] but is different in that we include spin-orbit interactions in the host material and at the impurity site. No attempts are made to use pseudopotentials here[13,47] as we will treat the potentials as adjustable parameters in our approach.

The introduction of an impurity potential in a substitutional way generally results in (1) an energy shift of the tightly bound impurity d levels, (2) a change in their coupling to the host bands, (3) a change in the scattering matrix of the nonresonant s and p waves incident at the impurity. Spherical waves of f and higher orbital quantum number are less affected, as they have only a small amplitude at the impurity site, due to the relatively high centrifugal barrier compared to the kinetic energies of the particles near E_F. A formal transformation of the Hamiltonian to the cubic double-point-group representations separates the s and p block from the d block of the Hamiltonian. We will concentrate mainly on the latter here, as the UPS spectra of transition metals are dominated by the d part of the density of states.

The Hamiltonian that we will solve is

$$H=H_{\text{host}}+\frac{1}{\sqrt{N}}\sum_{k}\sum_{\mu,\nu}[V_{k\mu}^{\nu}(C_{k\mu}^{\dagger}C_{0\nu}+C_{0\nu}^{\dagger}C_{k\mu})]$$
$$=H_{\text{host}}+\frac{1}{N}\sum_{k,q}\sum_{\mu,\nu}[(V_{k\mu}^{\nu}+V_{q\nu}^{\mu})C_{k\mu}^{\dagger}C_{q\nu}]\ , \tag{A1}$$

where ν and μ refer to double-point-group representations, k and q refer to momentum quantum numbers, and 0 refers to the impurity site.

We will first derive a general expression for the transition matrix of such a system, using the T-matrix Dyson equation $\mathbf{T}=\mathbf{V}+\mathbf{T}\mathbf{g}\mathbf{V}$, which reads in its explicit form:

$$T_{k\mu}^{k\nu}=\frac{1}{N}V_{k\mu}^{\nu}+\frac{1}{N}V_{q\nu}^{\mu}$$
$$+\frac{1}{N}\sum_{q'}\sum_{\nu',\nu''}[T_{k\mu}^{q'\nu'}g_{q'\nu'}^{q'\nu''}(V_{q\nu}^{\nu''}+V_{q'\nu''}^{\nu})]\ , \tag{A2}$$

where $g_{k\mu}^{k\nu}$ is the host-metal Green's function. In matrix notation, i.e., omitting the point-group indices and treating all quantities as operators, Eq. (A2) reads

$$\mathbf{T}_k^q=\frac{1}{N}\mathbf{V}_k+\frac{1}{N}\mathbf{V}_q^T+\frac{1}{N}\left[\sum_{q'}\mathbf{T}_k^{q'}\mathbf{g}_{q'}^{q'}\right]\mathbf{V}_q^T$$
$$+\frac{1}{N}\left[\sum_{q'}\mathbf{T}_k^{q'}\mathbf{g}_{q'}^{q'}\mathbf{V}_{q'}\right]\ . \tag{A3}$$

We solve this equation in terms of the known matrices:

$$\mathbf{L}\equiv\frac{1}{N}\sum_{q}(\mathbf{V}_q^T\mathbf{g}_q^q)\quad \mathbf{L}^T\equiv\frac{1}{N}\sum_{q}(\mathbf{g}_q^q\mathbf{V}_q)\ , \tag{A4}$$

$$\mathbf{M}\equiv\frac{1}{N}\sum_{q}(\mathbf{V}_q^T\mathbf{g}_q^q\mathbf{V}_q),\quad \mathbf{g}\equiv\frac{1}{N}\sum_{q}\mathbf{g}_q^q\ , \tag{A5}$$

and for the matrices we are seeking:

$$\mathbf{Y}_k\equiv\mathbf{1}+\sum_{q}(\mathbf{T}_k^q\mathbf{g}_q^q)\ , \tag{A6}$$

$$\mathbf{X}_k\equiv\mathbf{V}_k+\sum_{q}(\mathbf{T}_k^q\mathbf{g}_q^q\mathbf{V}_q)\ . \tag{A7}$$

Equation (A3) becomes with these definitions

$$\mathbf{T}_k^q=\frac{1}{N}(\mathbf{Y}_k\mathbf{V}_q^T+\mathbf{X}_k)\ , \tag{A8}$$

and can be solved using the resulting coupled equations:

$$\mathbf{Y}_k=\mathbf{1}+\mathbf{X}_k\mathbf{g}+\mathbf{Y}_k\mathbf{L}\ , \tag{A9}$$

$$\mathbf{X}_k=\mathbf{V}_k+\mathbf{Y}_k\mathbf{M}+\mathbf{X}_k\mathbf{L}^T\ , \tag{A10}$$

which are easily solved, resulting in

$$\mathbf{Y}_k=[\mathbf{V}_k(\mathbf{L}^T-\mathbf{1})^{-1}\mathbf{g}-\mathbf{1}]\mathbf{N}^{-1}\ , \tag{A11}$$

$$\mathbf{X}_k=[(\mathbf{L}-\mathbf{1})^{-1}\mathbf{M}-\mathbf{V}_k](\mathbf{N}^T)^{-1} \tag{A12}$$

with

$$\mathbf{N}\equiv(\mathbf{L}-\mathbf{1})-\mathbf{M}(\mathbf{L}^T-\mathbf{1})^{-1}\mathbf{g}\ . \tag{A13}$$

Inserting Eq. (A11) to (A13) in Eq. (A8), we finally find

$$\mathbf{T}_k^q=\frac{1}{N}[(\mathbf{L}-\mathbf{1})^{-1}\mathbf{M}-\mathbf{V}_k](\mathbf{N}^T)^{-1}$$
$$+\frac{1}{N}[\mathbf{V}_k(\mathbf{L}^T-\mathbf{1})^{-1}\mathbf{g}-\mathbf{1}]\mathbf{N}^{-1}\mathbf{V}_q^T\ . \tag{A14}$$

This equation only involves inversions of matrices of the rank of the number of bands taken into account. This becomes a trivial procedure in the one-band limit. We will discuss two limits next: first, where we neglect the degeneracy in the d bands, so that the problem reduces to the two-band limit, i.e., a d band and an sp band; and second, where we include the full d-band degeneracy, but where we assume a special form of the impurity potential.

2. First limit: nondegenerate d bands

The impurity part of the two band Hamiltonian reads

$$H_{\rm imp}=\frac{1}{N}\sum_{kq}[\Delta_k(d_k^\dagger d_q+d_q^\dagger d_k)+V_k(c_k^\dagger d_q+d_q^\dagger c_k)]\ , \tag{A15}$$

where $d^\dagger$ and $c^\dagger$ refer to d-band and sp-band creation operators, respectively. We use (A4) and (A5) to find the matrices L and M:

$$\mathbf{L}=\begin{bmatrix} l_d & l_s \\ 0 & 0 \end{bmatrix}\ , \tag{A16}$$

$$\mathbf{M}=\begin{bmatrix} \sigma_d+\sigma_s & 0 \\ 0 & 0 \end{bmatrix}\ , \tag{A17}$$

where the first rows and columns refer to the d index and the second rows and columns refer to the sp index of the matrices and where l_d, l_s, σ_d, and σ_s are defined as

$$l_d\equiv\frac{1}{N}\sum_q(\Delta_q g_{dq}^{dq}),\quad l_s\equiv\frac{1}{N}\sum_q(V_q g_{sq}^{sq})\ , \tag{A18}$$

$$\sigma_d\equiv\frac{1}{N}\sum_q[(\Delta_q)^2 g_{dq}^{dq}],\quad \sigma_s\equiv\frac{1}{N}\sum_q[(V_q)^2 g_{sq}^{sq}]\ . \tag{A19}$$

Using Eqs. (A13), (A16), and (A17), we find

$$\mathbf{N}^{-1}=D^{-1}\begin{bmatrix} l_d-1 & (l_d-1)l_s \\ 0 & -D \end{bmatrix}\ , \tag{A20}$$

where

$$D=(l_d-1)^2-(\sigma_s+\sigma_d)g_d^d\ . \tag{A21}$$

Using Eqs. (A14), (A16), (A17), and (A20), we find the transition matrix

$$\mathbf{T}_k^q=\frac{1}{ND}\begin{bmatrix} \Delta_k g_{d0}^{d0}\Delta_q+(1-l_d)(\Delta_k+\Delta_q)+\sigma_s+\sigma_d & \Delta_k g_{d0}^{d0}V_q+(1-l_d)V_q \\ V_k g_{d0}^{d0}\Delta_k+V_k(1-l_d) & V_k g_{d0}^{d0}V_q \end{bmatrix}\ . \tag{A22}$$

The Green's functions can be calculated easily using the relation

$$\mathbf{G}=\mathbf{g}+\mathbf{g}\mathbf{T}\mathbf{g}\ , \tag{A23}$$

so that the local impurity Green's function is

$$G_{d0}^{d0}=D^{-1}g_{d0}^{d0}\ , \tag{A24}$$

and the change in the total Green's function is

$$\mathrm{Tr}(G-g)=D^{-1}\left[\left[\frac{-\partial}{\partial\epsilon}\sigma_d\right]g_d^d+2(1-l_d)\left[\frac{-\partial}{\partial\epsilon}l_d\right]+(\sigma_s+\sigma_d)\left[\frac{-\partial}{\partial\epsilon}g_d^d\right]+\left[\frac{-\partial}{\partial\epsilon}\sigma_s\right]g_d^d\right]$$
$$=\frac{\partial}{\partial\epsilon}(\ln D)\ , \tag{A25}$$

where we used the property

$$[g_{k\mu}^{k\mu}(\epsilon)]^2=\frac{\partial}{\partial\epsilon}g_{k\mu}^{k\mu}(\epsilon)\ . \tag{A26}$$

From the definitions of l_d and σ_d we see that, generally, knowledge of the details of the host Green's functions is required to obtain the important denominator $D(\epsilon)$. We will show that such detailed information is not necessary in the limit of nearest-neighbor coupling only between d orbitals in the alloy and pure host metal. In this case the coupling parameter Δ_k occurring in Eq. (A15) reads in direct space representation:

$$\Delta_0^0=\tfrac{1}{2}\Delta,\quad \Delta_0^1=T,\quad \text{all other } \Delta_i^j=0\ , \tag{A27}$$

where Δ is the energy shift of the impurity d-state energy relative to the host d-band centroid and T is the change in coupling to nearest-neighbor d states at the impurity site: $T=T_{\rm host}^{\rm imp}-T_{\rm host}^{\rm host}$. Now let z be the nearest-neighbor coordination number, so that with Eqs. (A18) and (A19)

$$l_d=\tfrac{1}{2}\Delta g_{d0}^{d0}+zTg_{d0}^{d1}\ , \tag{A28}$$

and

$$\sigma_d=\tfrac{1}{4}\Delta^2 g_{d0}^{d0}+zT\Delta g_{d0}^{d1}+z^2T^2g_{d0}^{d1\pm1}\ , \tag{A29}$$

where g_{d0}^{d1} is the off-diagonal Green's function:

$$g_{d0}^{d1}=\frac{1}{N}\sum_{k}(g_{dk}^{dk}e^{ikR}) \tag{A30}$$

and R is in the first shell. In the case of nearest-neighbor coupling only g_{d0}^{d1} is related to g_{d0}^{d0} through the Dyson equation:[48]

$$(E-\bar{E}_d)g_{d0}^{d0}=1+T_{\rm host}^{\rm host}\sum_{R}g_{dR}^{d0}=1+zT_{\rm host}^{\rm host}g_{d0}^{d1}\ . \tag{A31}$$

The function

$$g_{d0}^{d1\pm1}=\frac{1}{z^2}\sum_{R,R'}(g_{d0}^{dR+R'})\ , \tag{A32}$$

where R and R' are in the first shell. The summation goes over z^2 values of $R+R'$ that are in the zeroth, first, second, or higher shells dependent on the topology of the host matrix. It is related to g_{d0}^{dR}, with R in the first shell, through the Dyson equation

$$(E-\bar{E}_d)g_{d0}^{dR}=T_{\rm host}^{\rm host}\sum_{R'}(g_{dR'}^{dR})=zT_{\rm host}^{\rm host}g_{d0}^{d1\pm1}\ , \tag{A33}$$

where R' is in the first shell. Insertion of Eqs. (A31) and (A33) in (A21), (A28), and (A29), and writing $t=T/T_{\rm host}^{\rm host}$, gives

$$D=(1+t)^2=\{[(1+t)^2-1](E-\bar{E}_d)+\Delta+\sigma_s\}g_{d0}^{d0}\ , \tag{A34}$$

and for the impurity local Green's function

$$G_{d0}^{d0}=\frac{g_{d0}^{d0}}{(1+t)^2-\{[(1+t)^2-1](E-\bar{E}_d)+\Delta+\sigma_s\}g_{d0}^{d0}}\ . \tag{A35}$$

This expression has two rather familiar limits.

(1) $t=-1$, where $\mathrm{Im}G_{d0}^{d0}$ is simply a lifetime broadened single line. Usually one replaces $\Delta+\sigma_s$ with an energy-independent complex energy, the imaginary part of which is the inverse decay time due to the s-d coupling.

(2) $t=0$, where we recognize the Clogston-Wolff formula[10] for the impurity DOS.

3. Second limit: local shift of the d states

The impurity Hamiltonian is

$$H_{\rm imp}=\sum_{\mu,\nu}(\Delta_{\mu}^{\nu}d_{0\mu}^{\dagger}d_{0\nu})+\frac{1}{\sqrt{N}}\sum_{k,\mu}[V_{k\mu}(c_{k\mu}^{\dagger}d_{0\mu}+d_{0\mu}^{\dagger}c_{k\mu})]\ . \tag{A36}$$

With Eqs. (A4) and (A5) and once again turning to matrix notation, we have

$$\mathbf{L}=\begin{bmatrix}1/2\Delta\mathbf{g}_d^d & \mathbf{l}_s\\ \mathbf{0} & \mathbf{0}\end{bmatrix}\ , \tag{A37}$$

$$\mathbf{M}=\begin{bmatrix}1/4\Delta\mathbf{g}_d^d\Delta & \mathbf{0}\\ \mathbf{0} & \mathbf{0}\end{bmatrix}\ , \tag{A38}$$

where the first row and column again refer to the d index and the second row and column to the sp index, but now contain block matrices of rank 10. Using Eqs. (A13), (A37), and (A38), we find

$$\mathbf{N}^{-1}=\begin{bmatrix}(1/2\Delta\mathbf{g}_d^d-1)\mathbf{D}^{-1} & (\Delta\mathbf{g}_d^d-1)\mathbf{D}^{-1}\mathbf{l}_s\\ \mathbf{0} & -1\end{bmatrix} \tag{A39}$$

with

$$\mathbf{D}=\mathbf{1}-(\Delta+\sigma_s)\mathbf{g}_d^d\ . \tag{A40}$$

With Eqs. (A14), (A37), (A38), and (A39) we find

$$\mathbf{T}_k^q=\frac{1}{N}\begin{bmatrix}\mathbf{D}^{-1}(\Delta+\sigma_s) & \mathbf{D}^{-1}\mathbf{V}_q\\ \mathbf{V}_k(\mathbf{D}^T)^{-1} & \mathbf{V}_k\mathbf{g}_d^d\mathbf{D}^{-1}\mathbf{V}_q\end{bmatrix}\ . \tag{A41}$$

The local impurity Green's function can be found with a little algebra:

$$G_{d0\mu}^{d0\mu'}=g_{d0\mu}^{d0\mu'}+\sum_{q,q'}\sum_{\nu,\nu'}(g_{d0\mu}^{q\nu}T_{q\nu}^{q'\nu'}g_{q'\nu'}^{d0\mu})=\sum_{\mu''}[g_{d0\mu}^{d0\mu''}(D^{-1})_{\mu''}^{\mu'}]\ . \tag{A42}$$

The change in the total Green's function is

$$\begin{aligned}\mathrm{Tr}(\mathbf{G}-\mathbf{g})&=\sum_{\substack{\mu,\mu'\\ \nu,\nu'}}\sum_{k}[g_{dk\mu}^{dk\mu'}(D^{-1})_{\mu'}^{\nu}(\Delta+\sigma_s)_{\nu}^{\nu'}g_{dk\nu'}^{dk\mu}]\\ &\quad+\sum_{\mu,\mu'}\sum_{k}[g_{sk\mu}^{sk\mu}V_{k\mu}g_{d0\mu}^{d0\mu'}(D^{-1})_{\mu'}^{\mu}V_{k\mu}g_{sk\mu}^{sk\mu}]\\ &=-\sum_{\substack{\mu,\mu'\\ \nu}}\left[(D^{-1})_{\mu}^{\nu}\frac{\partial}{\partial\epsilon}[g_{d0\mu'}^{d0\mu}(\Delta+\sigma_s)_{\nu}^{\mu'}]\right]\\ &=\frac{\partial}{\partial\epsilon}\mathrm{Tr}(\ln\mathbf{D})\ .\end{aligned} \tag{A43}$$

The change in the UPS spectrum is found as explained in the Appendix of Ref. 15 by replacing the Green's function in the numerator with the *experimental* one:

$$\rho_{\rm alloy}-\rho_{\rm host}=-\pi^{-1}\mathrm{Im}\left[D^{-1}\frac{\partial}{\partial\epsilon}(g_{\rm expt})(\Delta+\sigma_s)\right]\ . \tag{A44}$$

4. Scattering phase shifts

There exists a useful relation between the difference in the total DOS and the transition matrix, often employed in the Friedel sum rule in the context of free-electron scattering. Because the T matrix satisfies the optical theorem,

$$\mathrm{Im}\mathbf{T}=\mathbf{T}^{T}(\mathrm{Im}g)\mathbf{T}\ , \tag{A45}$$

the S matrix defined as

$$\mathbf{S}=\mathbf{1}+2i(\mathrm{Im}g)\mathbf{T} \tag{A46}$$

is unitary: Here Img ensures energy conservation, or on energy shell scattering. Near the Fermi level the d-band DOS is zero, so that only scattering between s-p states occur. In that case the S matrix has a particular transpar-

ent form, namely

$$S_\mu = e^{2i\eta_\mu} , \tag{A47}$$

where the basis μ has been chosen such, as to diagonalize S. In the absence of spin-orbit symmetry mixing, these are just the cubic harmonics e_g and t_{2g}. Spin-orbit splitting splits the basis in the representations $\Gamma_7, \Gamma_{8'}$, and $\Gamma_{8''}$, where $\Gamma_{8'}$ and $\Gamma_{8''}$ mix as a function of energy. Nevertheless, one can choose the basis such that S is diagonal near E_F, which is useful only if the symmetry mixing does not vary too much near E_F. Therefore, we have

$$[\mathrm{Im} g^{s\mu}_{s\mu}(E)] T^{k\mu}_{k\mu}(E) = (\sin\eta_\mu) e^{i\eta_\mu} , \tag{A48}$$

or, with Eq. (A22) or (A41),

$$\eta_\mu(E) = \mathrm{Arg}[T^{k\mu}_{k\mu}(E)] = \mathrm{Im}(\ln D^\mu_\mu) , \tag{A49}$$

so that, with Eq. (A25) or (A43),

$$\frac{\partial \eta_\mu(E)}{\partial E} = \mathrm{Im}(G^\mu_\mu - g^\mu_\mu) . \tag{A50}$$

In other words, the energy derivatives of the scattering phase shifts equal the changes in the total density of states in the energy regions *outside* the host d band.

---

*Present address: Philips Research Laboratories, 5600 JA Eindhoven, The Netherlands.

[1]J. Friedel, Nuovo Cimento Suppl. **7**, 287 (1958).

[2]P. W. Anderson, Phys. Rev. **124**, 41 (1961).

[3]Grüner and Zawadowski, Rep. Prog. Phys. **37**, 1497 (1974).

[4]A. Bosch, H. Feil, G. A. Sawatzky, and J. A. Julianus, J. Phys. F **14**, 2225 (1984).

[5]P. J. Braspennig, R. Zeller, A. Lodder, and P. H. Dederichs, Phys. Rev. B **29**, 703 (1984).

[6]J. S. Faulkner and G. M. Stocks, Phys. Rev. B **21**, 3222 (1980).

[7]G. M. Stocks and H. Winter, Z. Phys. B **46**, 95 (1982).

[8]H. Winter, P. J. Durham, and G. M. Stocks, J. Phys. F **14**, 1047 (1984).

[9]A. J. Pindor, W. M. Temmerman, B. L. Gyorffy, and G. M. Stocks, J. Phys. F **10**, 2617 (1980).

[10]A. M. Clogston, B. T. Matthias, M. Peter, H. J. Williams, E. Corenzwit, and R. J. Sherwood, Phys. Rev. **125**, 541 (1962).

[11]B. Velicky, S. Kirkpatrick, and M. Ehrenreich, Phys. Rev. **175**, 747 (1968).

[12]R. Riedinger, J. Phys. F **1**, 392 (1971).

[13]F. Gautier, J. Phys. F **1**, 382 (1971).

[14]D. van der Marel, G. A. Sawatzky, and F. U. Hillebrecht, Phys. Rev. Lett. **53**, 206 (1984).

[15]D. van der Marel, C. Westra, G. A. Sawatzky, and F. U. Hillebrecht, Phys. Rev. B **14**, (1985).

[16]J. A. Julianus, A. Myers, F. F. Bekker, D. van der Marel, and E. F. Allen, J. Phys. F **15**, 111 (1985).

[17]A. Bosch, H. Feil, and G. A. Sawatzky, J. Phys. E **17**, 1187 (1984).

[18]D. E. Eastman, J. A. Knapp, and F. J. Himpsel, Phys. Rev. Lett. **41**, 825 (1978).

[19]The *Au*Pd (4.5 at. %), *Au*Pt (4.5 at. %), *Ag*Pd (3 at. %), and *Ag*Pt (2 at. %) samples were supplied by Dr. A. Myers and co-workers for which we want to express our gratitude.

[20]J. L. Gardner and J. A. R. Samson, J. Electron Spectrosc. Relat. Phenom. **6**, 53 (1975).

[21]A. D. McLachlan, J. G. Jenkin, R. C. G. Leckey, and J. Liesegang, J. Phys. F **5**, 2415 (1975).

[22]D. van der Marel, G. A. Sawatzky, and J. A. Julianus, J. Phys. F **14**, 281 (1984).

[23]S. Hüfner, G. K. Wertheim, and J. H. Wernick, Solid State Commun. **17**, 1585 (1975).

[24]N. Mårtensson, R. Nyholm, M. Calén, and J. Hedman, Phys. Rev. B **24**, 1725 (1981).

[25]R. S. Rao, A. Bansil, H. Asonen, and M. Pessa, Phys. Rev. B **29**, 1713 (1984).

[26]G. S. Sohal, R. G. Jordan, and P. J. Durham, Surf. Sci. **152**, 205 (1985).

[27]C. Norris and L. Walldén, Solid State Commun. **7**, 99 (1969).

[28]V. V. Nemoshalenko, M. G. Chudinov, V. G. Aleshin, Y. N. Kucherenko, and L. M. Sheludchenko, Solid State Commun. **16**, 755 (1975).

[29]C. R. Helms and D. Collins, Solid State Commun. **17**, 459 (1975).

[30]G. G. Kleiman, V. S. Sundaram, and M. B. de Moraes, Phys. Rev. B **23**, 3177 (1981).

[31]C. Norris and P. D. Nilsson, Solid State Commun. **6**, 649 (1968).

[32]P. Weightman and P. T. Andrews, J. Phys. C. **13**, L815 (1980).

[33]S. Hüfner and G. K. Wertheim, Phys. Lett. **51A**, 299 (1975).

[34]E. Antonides and G. A. Sawatzky, *Proceedings of the International Conference on the Physics of Transition Metals, Toronto, 1977,* edited by M. J. G. Lee, J. M. Perz, and E. Fawcett (IOP, London, 1978), p. 134.

[35]N. V. Smith, Phys. Rev. B **3**, 1862 (1971); N. V. Smith, G. K. Wertheim, S. Hüfner, and M. M. Traum, Phys. Rev. B **10**, 3197 (1974).

[36]R. Zeller and P. J. Braspennig, Solid State Commun. **42**, 701 (1982).

[37]J. A. Julianus, F. F. Bekker, and P. F. de Châtel, J. Phys. F **14**, 2061 (1984); **14**, 2077 (1984).

[38]E. F. Bekker and N. Zuiderbaan, Physica **85B**, 113 (1976).

[39]A. B. Callender and S. E. Schnatterly, Phys. Rev. B **7**, 4385 (1973).

[40]G. M. Stocks, W. M. Temmerman, and B. L. Gyorffy, Phys. Rev. Lett. **41**, 339 (1978).

[41]P. Weightman, P. T. Andrews, G. M. Stocks, and M. Winter, J. Phys. C **16**, L81 (1983).

[42]M. Davies and P. Weightman, J. Phys. C **17**, L1015 (1984).

[43]M. Vos, D. van der Marel, and G. A. Sawatzky, Phys. Rev. B **15**, 3073 (1984).

[44]M. Vos, G. A. Sawatzky, P. Weightman, and P. T. Andrews, Solid State Commun. **52**, 159 (1984).

[45]J. Stöhr, G. Apai, P. S. Wehner, F. R. McFeely, R. S. Williams, and D. A. Shirley, Phys. Rev. B **14**, 5144 (1976).

[46]N. E. Christensen, J. Phys. F **8**, L51 (1978).

[47]P. V. Smith, J. Phys. F **11**, 1207 (1981).

[48]This relation holds for tight-binding Hamiltonians where only nearest-neighbor atoms are coupled. The reader can check this from Eqs. (5.15) and (5.21) in Chap. 5 of E. N. Economou, *Green's Functions in Quantum Physics,* Vol. 7 of *Springer Series in Solid State Physics,* edited by M. Cardona, P. Fulde, and H. J. Queisser (Springer, Berlin, 1983).